ELSEVIER

Ceramics International 29 (2003) 725–734

CERAMICS INTERNATIONAL

www.elsevier.com/locate/ceramint

Effect of substrate temperature on structural, electrical and optical properties of sprayed tin oxide (SnO_2) thin films

P.S. Patil[a,*], R.K. Kawar[a], T. Seth[b], D.P. Amalnerkar[b], P.S. Chigare[a]

[a]*Thin Film Physics Laboratory, Department of Physics, Shivaji University, Kolhapur-416 004, India*
[b]*Center for Materials for Electronics Technology (C-MET), Off. Pashan Road, Panchavati, Pune-411 008, India*

Received 4 April 2002; received in revised form 9 September 2002; accepted 15 November 2002

Abstract

The thin films of undoped tin oxide (SnO_2) were deposited onto the amorphous glass substrates using a pneumatic spray pyrolysis technique (SPT). The films were deposited at various substrate temperatures ranging from 300 to 500 °C in steps of 50 °C. The effect of substrate temperature on structural, electrical and optical properties was studied. The thermal behavior of the precursor $SnCl_4{\cdot}5H_2O$ is described in the results of thermo gravimetric analysis (TGA) and differential thermal analysis (DTA). Infrared (IR) spectroscopic studies reveal that the strong vibration band characteristic of SnO_2 stretching is present around 620 cm^{-1}. The Raman spectrum of SnO_2 films indicated bonding between Sn and O_2 at 580 cm^{-1}. The X-ray diffraction study showed that all the films were polycrystalline with major reflex along (110) plane, manifested with amelioration of grain size at an elevated substrate temperature. The films deposited at 450 °C exhibited lowest resistivity (0.7 Ω cm) and consequently highest n-type conductivity among all the samples. The direct band gap energy was found to vary from 3.62 to 3.87 eV and transmittance at 630 nm varies from 73 to 85% with a rise in substrate temperature.

Keywords: Tin oxide; Thin films; Spray pyrolysis technique (SPT); Characterization

1. Introduction

Tin oxide is a multifaceted material having uses in optical technology [1], consequently leading to almost impenetrable literature [2]. Tin oxide thin films have been successfully demonstrated as transparent conductors (TC), optical windows for the solar spectrum, stability resistors, touch-sensitive switches, digital displays, light emitting diodes (LEDs), electrochromic displays (ECDs), and many more [3–5], mainly due to their outstanding properties.

The consensus of the researchers is that for TC, high transmittance (T%) and relatively low electrical resistivity (ρ) is desirable while for applications such as display devices and LEDs, low electrical resistivity is desirable and not high transmittance [6]. These applications rely on itinerant electrons that stem from the ionization of the dopants and enter the conduction band. For ECDs, which hinges on the ability of the material to sustain mixed conduction of ions and electrons, low electrical resistivity is more desirable than high transmittance [7,8], additionally it is useful to have some water content in the resultant film [1,4], which plays key role in inducing electrochromic (EC) effect.

It is noticed from the literature survey that the variety of methods of preparation will lead to the layers having different optical and electrical properties, which evokes critical influence of oxygen vacancies, serving as donor in tin oxide films [9,10]. In principle physical methods viz. sputtering [1,5], and thermal evaporation [11], lead to weakly non-stoichiometric tin oxide with co-existence of other insulating phases like SnO, resulting into relatively high resistive films. The range of resistivity in as-deposited SnO_x films typically varies from 6.6×10^{-3} to 2.5×10^{-3} Ω cm [5]. On the other hand chemical methods especially spray pyrolysis technique, lead to strongly non- stoichiometric tin oxide films without co-existence of insulating phases, resulting into comparatively low resistive films [6,12–19]. The electrical resistivity in as-deposited SnO_x films typically varies from 1.45×10^{-3} Ω cm to 0.45×10^{-3} Ω cm, which is several times less than

* Corresponding author.
E-mail address: patilps_2000@yahoo.com (P.S. Patil).

0272-8842/03/$30.00
doi:10.1016/S0272-8842(02)00224-9

the films deposited by physical methods. Therefore, it can be concluded that the SnO_x films deposited by spray pyrolysis technique are more susceptible to oxygen deficiencies [13,14,16,18,19].

We are interested in SnO_x films in connection with the electrochromism. Electrochromic tin oxide films were described recently by Orel et al. [7] and Olivi et al. [8] who prepared their samples by dip-coating and Isidorosson et al. [1] by sputtering and emphasize the importance of various properties that SnO_x should exhibit for attaining pronounced electrochromism. In this investigation, we have employed spray pyrolysis technique for SnO_x thin film deposition and discussed their structural, electrical and optical properties. The deposition has been carried out from aqueous stannic chloride solution, with a postulation that the resultant films may have some water content [1,4], which would be in turn beneficial for better electrochromic effect. Several experiments on electrochromism in SnO_x thin films are underway and results will be disseminated elsewhere.

2. Experimental

The tin oxide films were prepared by using pentahydrated stannic chloride ($SnCl_4.5H_2O$) aqueous solution as a precursor. By using double distilled water, 0.1 M stannic chloride solution was prepared and sprayed through specially designed glass nozzle of 0.5 mm inner diameter onto the ultrasonically cleaned amorphous glass substrates. The deposition parameters like solution concentration (0.1 M), rate of spraying solution (5 cc min^{-1}) nozzle to substrate distance (28 cm), pressure of carrier gas (1 kg cm^{-2}) and to and fro frequency of the nozzle (15 cycles min^{-1}) were kept constant at the optimized values indicated in brackets. The substrate temperature was varied from 300 to 500 °C in steps of 50 °C using electronic temperature controller, model 9601 (Aplab make) with an accuracy of ± 5 °C. The Chromel-Alumel thermocouple was used to measure the temperatures of the hot plate. The films prepared at 300, 350, 400, 450 and 500 °C are denoted by S1, S2, S3, S4 and S5, respectively. All the films were transparent, adherent to the substrates, uniform, pinhole free and stable for long period when kept in the atmosphere.

The films were characterized by means of structural, electrical and optical techniques. To select the range of substrate temperature for deposition, thermo gravimetric analysis (TGA) and differential thermal analysis (DTA) of stannic chloride ($SnCl_4{\cdot}5H_2O$, A.R grade purity 97%) was carried out using TA instrument (USA) STD 2960 (simultaneous DSC–TGA). The powder scratched from deposited films was characterized by Infrared (IR) spectroscopy using Perkin Elmer IR spectrometer model 783 in the spectral range 200–4000 cm^{-1}. To record IR patterns, the pellets were prepared by mixing KBr with tin oxide powder collected by scratching thin films from glass substrates in the ratio 300:1 and then pressing powder between two pieces of polished steel. All the samples of tin oxide were characterized by specially resolved Raman scattering using 150 mW at laser head and 4 mW on the sample of 514.5 nm line of an argon ion laser. The scattered light was dispersed through the JY-T64000 Triple Monochromator System and detected with a liquid nitrogen cooled, high resolution charge coupled device (CCD) detected in the Z (XX) Z back scattering geometry. The size of the laser spot on the sample is 1.2 μm with 100 X objectives.

The structural properties of the films were studied by a Philips PW 3710 X-ray diffractometer using CuK_α radiation of wavelength 1.5405 Å operated at 25 kV, 20 mA. The scanning electron micrographs (SEMs) were carried out by Philips Make XL series, XL 30. The thickness of the film was measured using weight difference method by considering bulk density of the material (6.95 mg/cc). The electrical resistivity was determined by means of two point probe method in the temperature range of 300–575 K with ± 5 K accuracy. The Seebeck measurements were carried out with the help of thermoelectric power (TEP) unit in the temperature range of 300–575 K with ±5 K accuracy. The optical absorption and transmittance were studied with UV–vis-NIR spectrophotometer, Hitachi model 330 in the wavelength range of 300–850 nm at room temperature.

3. Results and discussion

3.1. Thermal decomposition characteristic of stannic chloride, ($SnCl_4{\cdot}5H_2O$)

The thermal decomposition behaviors of the precursor, $SnCl_4{\cdot}5H_2O$ were studied using TG and DT analyses techniques. TGA and DTA were performed from 45 to 800 °C with alumina as a reference material at the scan rate of 10 °C per minute. The DTA chamber was purged with an ambient air at the flow rate of 100 cm^3/min. The TGA and DTA thermograms obtained for $SnCl_4{\cdot}5H_2O$ are shown in Fig. 1(a and b). The thermal evolution in air takes place in six consecutive stages with weight losses for which inflection points coincide with the temperature corresponding to exothermic and endothermic peaks in DTA trace. The weight loss of the precursor begins as heat is applied at 45 °C. It is clearly depicted that the loss of water from the precursor take place at various temperatures, 70, 100, 140 and 150 °C, corresponding to which endothermic peaks were observed. The total weight loss corresponding to removal of both the physisorbed and chemisorbed water of crystallization ($5H_2O$) is calculated to be about 87%. The regular weight loss commences at about 170 °C,

which is the indication of onset of the thermal decomposition of the precursor. This regular weight loss continues up to 450 °C. During this temperature range, the weight loss is mainly due to the expulsion of Cl^- ions form the precursor, which leads to the formation of non-stoichiometric tin oxide. After 450 °C, the rate of weight loss is very slow up to 700 °C. This evinces that at 450 °C, transformation of non-stoichiometric tin oxide to nearly stoichiometric tin oxide takes place. This process of transformation continues up to about 700 °C. It is difficult to calculate exact degree of non-stoichiometry from present analysis. Beyond 700 °C no further weight loss takes place to up to 850 °C, indicating formation of stoichiometric SnO_2 at 700 °C.

3.2. Film formation and thickness measurement

3.2.1. Film formation

Stannic chloride solution was sprayed on to the preheated amorphous glass substrates through specially designed glass nozzle. The sprayed droplets undergo evaporation, solute condensation and thermal decomposition thereby resulting in the formation of tin oxide thin films.

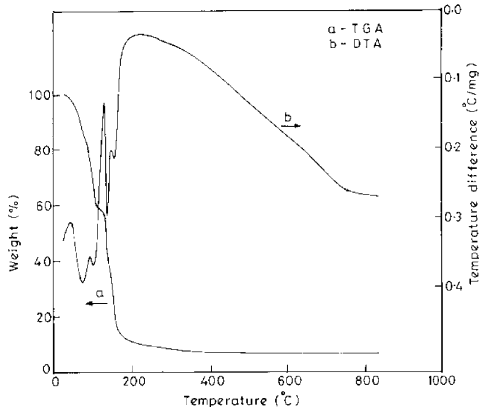

Fig. 1. (a) Thermal gravimetric analysis (TGA) and (b) differential thermal analysis (DTA) of the precursor powder of stannic chloride salt ($SnCl_4 \cdot 5H_2O$) in the temperature range 25–850 °C.

3.2.2. Thickness measurement

Thickness of the deposited films was measured by using weight difference method. The relation (1) was used to deduce the film thickness (t),

$$t = \frac{m}{\rho A} \tag{1}$$

where m is the mass of the film deposited on area A and ρ is the bulk density of the material. The values of thickness obtained by this method are listed in Table 1.

It is noted that film thickness decreases from 0.95 to 0.4 μm with rise in substrate temperature. The rise in substrate temperature increases evaporation rate of initial product leading to diminish mass transport towards the surface of the hot substrates resulting into the decrement in the film thickness. The actual values of film thickness would slightly be higher as the film density is certainly not equal to the bulk density, considered for the film thickness calculations.

3.3. Infrared spectroscopy (IR)

The IR transmittance spectrum presents information about phase composition as well as the way oxygen is bound to the metal ions (M–O structure). IR transmittance spectra of the powder scratched from the samples in the wavelength range 200–4000 cm^{-1} are shown in Fig. 2.

The spectrum for sample S1 comprises seven transmission bands at 580 cm^{-1} (ν_1), 620 cm^{-1} (ν_2), 1020 cm^{-1} (ν_3), 1370 cm^{-1} (ν_4), 1400 cm^{-1} (ν_5), 1600 cm^{-1} (ν_6) and 3460 cm^{-1} (ν_7). The ν_1 and ν_2 bands correspond to Sn–O and Sn–O_2 stretching, respectively. The bands ν_3, ν_4 and ν_5 can be assigned to chloride (Cl^-) ions retained in the film, since the film under investigation is prepared at lower substrate temperature (300 °C). The water bending vibrations have produced ν_6 (H–OH stretching) and ν_7 (physisorbed water) bands. The inclusion of water molecules might be due to (i) water of crystallization retained in the sample as deposition temperature was 300 °C; (ii) absorption of water during mixing and pelleting with KBr and (iii) entrapment of

Table 1
Effect of substrate temperature on properties of tin oxide thin films prepared by spray pyrolysis technique

Sample no.	Substrate temperature (°C)	Thickness (μm)	Grain size (Å)	Room temperature resistivity (ρ_{RT}, Ω cm)	Thermo emf (μV/°C)	Donor activation energy		Band gap energy (eV)	T% at 630 nm
						Region I (eV)	Region II (eV)		
S1	300	0.95	39	4.4	45	0.008	0.16	3.62	73
S2	350	0.90	42	2.6	36	0.008	0.15	3.84	78
S3	400	0.78	55	1.1	31	0.008	0.11	3.86	79
S4	450	0.59	59	0.7	22	0.008	0.10	3.87	82
S5	500	0.40	65	1.7	16	0.008	0.13	3.85	85

water vapour during spray deposition. Analogous result is reported by Senguttuvan et al. [20]. The I.R. spectrum for the S2 sample depicts that the bands due to Cl^- ions (ν_3, ν_4 and ν_5) became feeble and disappeared completely above it. Moreover the ν_6 and ν_7 bands get weakened appreciably at and above 400 °C, although cannot be completely alleviated. This indicates that the samples deposited below 400 °C (S1 and S2) do contain Cl^- ion contamination and are hydrated, while those deposited at and above it (S3, S4 and S5) are devoid of Cl^- ion contamination and are relatively less hydrated.

The O/Sn ratio was estimated from energy dispersive analysis by X-ray spectroscopy (EDAX) technique. It was about 1.7 for samples S3, S4 and S5 and about 1.6 for S1 and S2 samples.

3.4. Raman spectroscopy

This spectroscopy gives information on Sn–O_2 bonding Fig. 3 shows Raman spectrum for S1 sample. The broad peak at ~580 cm^{-1} is associated with tin-oxygen (Sn–O) stretching mode. Absorption at ~1090 cm^{-1} has been ascribed to stretching vibration mode terminal Sn–O_2 bands. These results are consistent with the results obtained in IR spectroscopy.

3.5. X-ray diffraction studies

The XRD patterns of all the films prepared at different substrate temperatures are shown in Fig. 4. It is found that all the tin oxide films are polycrystalline in nature and are of a cassiterite tetragonal (rutile type) structure with a major reflex along (110) plane. Other phases like β-SnO, α-SnO, Sn_2O_3, Sn_3O_4, etc., are not observed. The preferred orientation remains along (110) plane for all the samples S1, S2, S3, S4 and S5 irrespective of the substrate temperature and consequently the film thickness. Other planes corresponding to (101), (200), (211), (220), (310) and (301) also appeared with weak intensities. Similar results have been reported for spray deposited tin oxide (SnO_2) films by Vasu et al. [15] and for evaporated SnO_2 films by Das et al. [10]. Czapla et al. [9] have reported for evaporated tin oxide (SnO_2) films that other low intensity peaks of the films diminished at the substrate temperature above 400 °C and the (110) plane became the strongest under the condition of varying substrate temperature of the films.

The d values (interplaner spacings) of XRD reflections shown in Fig. 4 were estimated and compared with the standard d values taken from Joint Commission for Powder Diffraction Standards (JCPDS) data, card No.41-1445. The observed *d* values were in good agreement with the standard *d* values, confirming that the material deposited is SnO_2. The observed and standard *d* values are listed in Table 2. It is manifested that as the substrate temperature increases, the intensity corresponding to major (110) plane gets enhanced, which shows that the films deposited at higher temperatures have better crystallinity.

It is conceived that the tin oxide films deposited by physical techniques like, sputtering, electron beam evaporation, and thermal evaporation consist of mixed

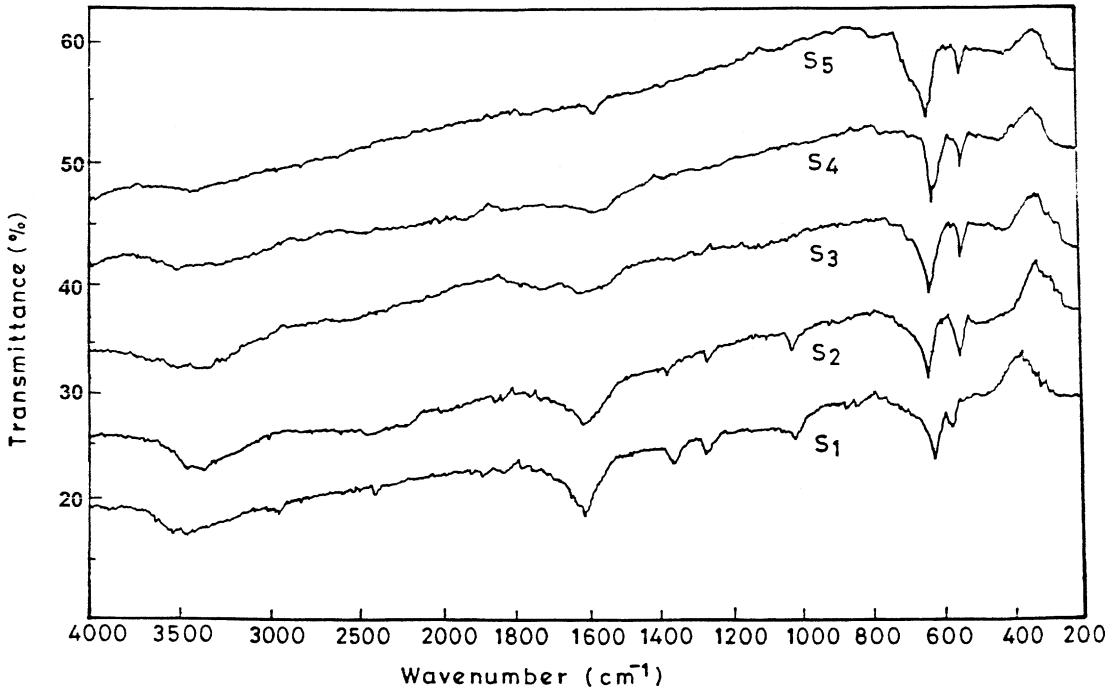

Fig. 2. IR spectra of all the samples of tin oxide thin films deposited at various substrate temperatures, S1 (300 °C), S2 (350 °C), S3 (400 °C), S4 (450 °C) and S5 (500 °C).

phases of β-SnO, α-SnO, Sn_2O_3 [10,11,21,22]. It is also observed that the films deposited at low substrate temperature (~150 °C), with a higher initial value of x in SnO_x, take up the crystalline structure of SnO_2 more easily upon annealing [11]. However, the tin oxide films deposited by spray pyrolysis technique using aqueous and non-aqueous $SnC1_4{\cdot}5H_2O$ precursor solutions consist of SnO_2 phase only. The preferred orientation of the crystallites was reported to be along (110) plane for SnO_2 films derived from lower concentration (below 0.1 M) of aqueous $SnC1_4{\cdot}5H_2O$ precursor solution with small crystallite size [23] and that along (200) plane for the films derived from higher concentration (above 0.1 M) of non-aqueous $SnC1_4{\cdot}5H_2O$ precursor solution with larger crystallite size [16,17]. The X-ray results in this investigation matches well with the literature results [12].

In order to determine the crystallite size, a slow scan of XRD pattern between 25 and 27° (since major reflex is found in this range) was carried out with the step 0.02°/min for all the samples. The size of the crystallites oriented along (110) plane can be deduced using Scherrer's formula (2), [24].

$$D = \frac{0.9\lambda}{\beta.\cos\theta} \tag{2}$$

where D is the size of crystallite, β is the broadening of diffraction line measured at half its maximum intensity in radians and λ is the wavelength of X-rays (1.5405 Å). Here, we presume that values of angle θ, β and instrumental error are common for all samples. The calculated values of crystallite size for all the samples are given in Table 1. From the values of crystallite size, it is found that the grain size increases from 39 to 65 Å with increase in substrate temperature 300–500 °C. This may be due to the fact that the smaller crystallites have surfaces with sharper convexity. This provides larger area of contact between adjacent crystallite, facilitating coalescence process to from larger crystallites [25].

3.6. Scanning electron microscopy (SEM) and electrical resistivity

Fig. 5(a–d) shows SEMs of the S1, S2, S3 and S4 samples, respectively, with ×10,000 magnification. It is observed that samples S1 has more asperity (rough surface morphology) than other samples and no well defined crystallites can be seen, which renders higher room temperature electrical resistivity (ρ_{RT}) in it. Sample S2 has more uniform surface than S1, which is probably responsible for their slightly lower value of room temperature electrical resistivity ρ_{RT}. Upon further rise in the deposition temperature (sample S3 deposited at 400 °C), the film surface became highly smooth with more uniformity and devoid of pin-holes. Some spherical shaped grains have started forming on the surface. This might have decreased grain boundary scattering and resulted into lowering of room temperature electrical resistivity than that of S2 sample. The sample S4, which was deposited at 450 °C consists of uniform distribution of spherical grains with relatively higher density, there by minimizing the grain boundary scattering. The crystallite size was estimated to be 59 Å.

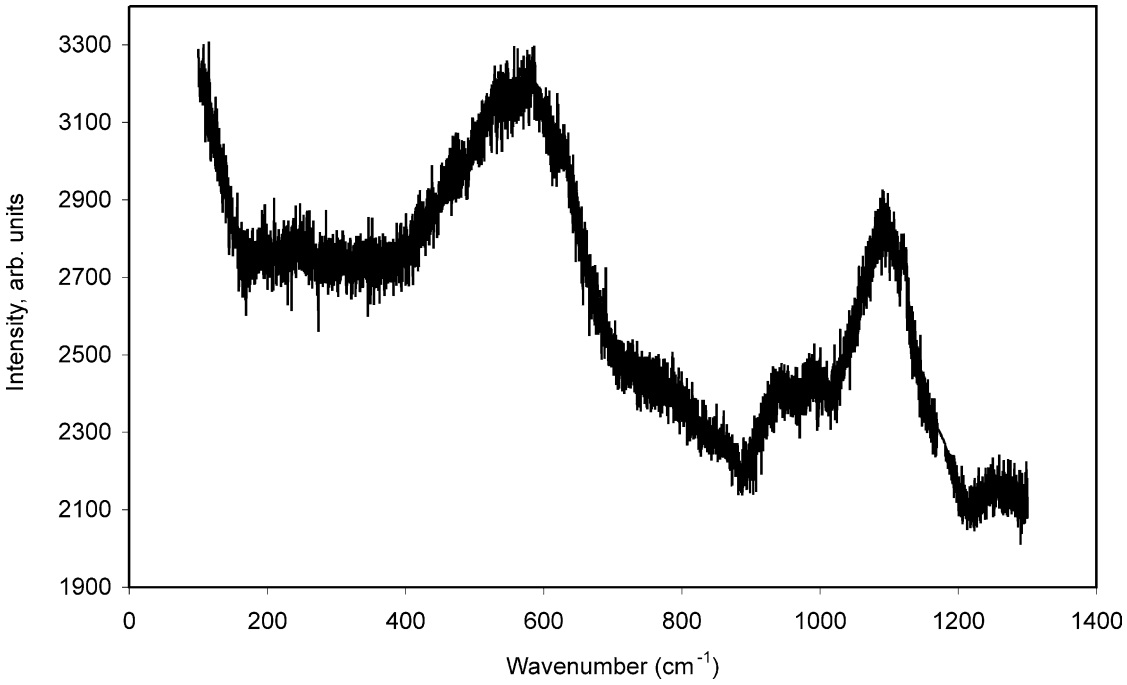

Fig. 3. The Raman spectrum of the S1 (300 °C) sample of tin oxide thin film.

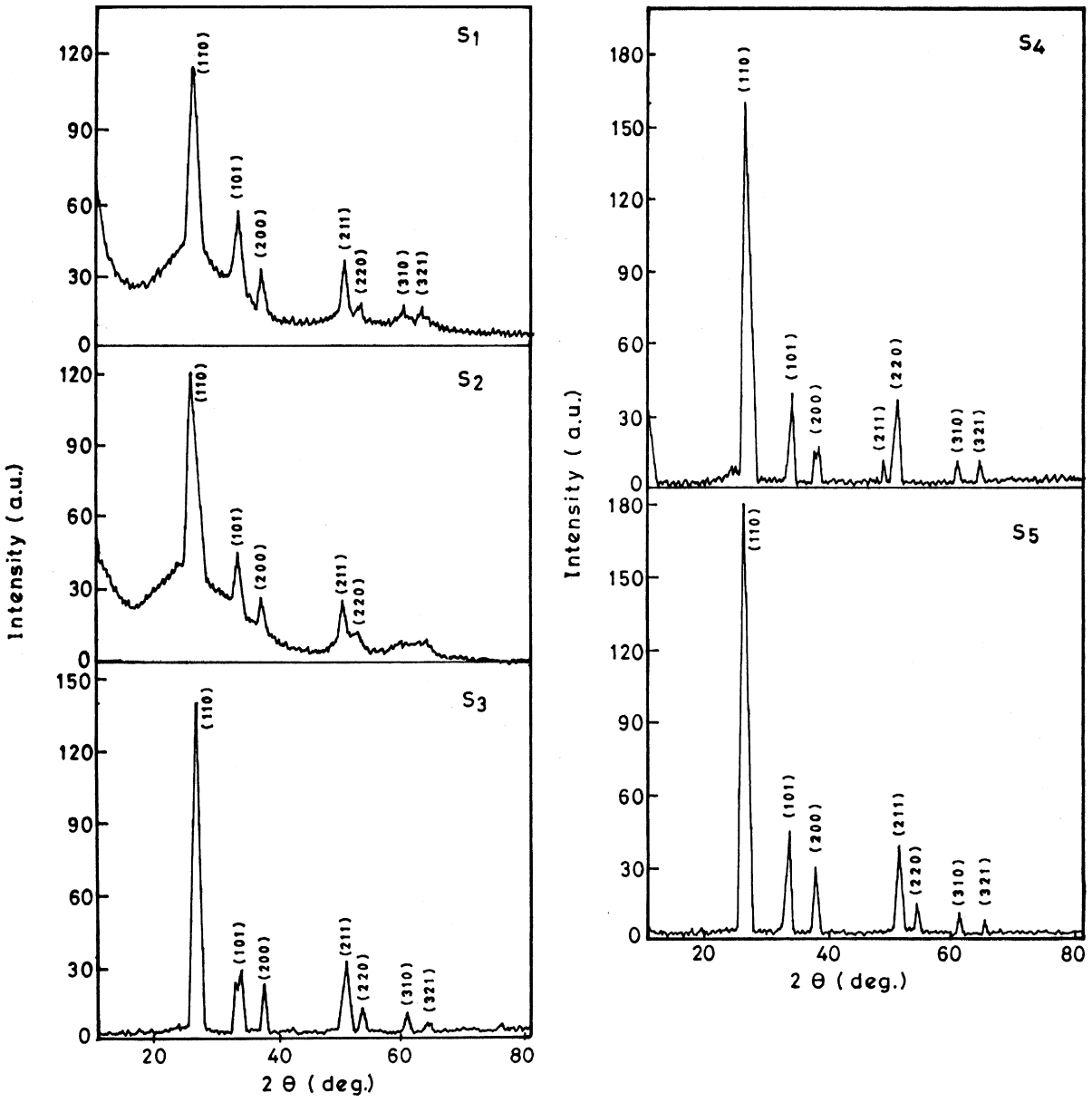

Fig. 4. The XRD patterns of SnO_2 thin films deposited at various substrate temperatures, S1 (300 °C), S2 (350 °C), S3 (400 °C), S4 (450 °C) and S5 (500 °C).

Table 2.
Comparison of the observed and standard d values of tin oxide thin films prepared at various substrate temperatures

Standard *d* values (Å)	Observed *d* values for samples (Å)					
	S1	S2	S3	S4	S5	(hkl) plane
3.3470	3.3570	3.3415	3.3527	3.3438	3.3515	(110)
2.6427	2.6414	2.6234	2.6463	2.6278	2.6507	(101)
2.3690	2.3684	2.3780	2.3699	2.3609	2.3820	(200)
1.7641	1.7738	1.7622	1.7665	1.7600	1.7665	(211)
1.6750	–	1.6802	1.6744	1.6761	1.6816	(220)
1.4984	1.4949	1.5000	1.4969	1.4968	1.5005	(310)
1.4155	1.4042	1.4193	1.4233	1.4206	–	(301)

The sample is completely devoid of asperity and pin - holes. Thus sample S4 has lowest room temperature resistivity among all other samples. The XRD results echo above findings, as well. Thus the thermal energy produced at 450 °C deposition temperature at given solution concentration (0.1 M) is sufficient enough to enforce the thin layers to grow more uniformly with fine grain structure and consequently become more conductive. Further increase in crystallite's size (65 Å) is observed at 500 °C deposition temperature (samples S5; SEM not shown). It also has higher crystallinity as evidenced by XRD results. However, its room temperature resistivity (ρ_{RT}) is slightly higher than S4 sample. It is concluded that the asperity in tin oxide thin films wanes with deposition temperature, which in turn induces higher conductivity, at 450 °C being maximum. Sample S5 has better crystallinity among others samples but exhibit relatively higher resistivity. In this case two mechanisms compete. While the ordering of the structure leads to a less resistant film, the oxidation draws the SnO_x near to its stoichiometric oxide, i. e. diminishes its defects which are responsible for the conductivity; increasing the film resistance. Pure stoichiometric undoped SnO_2 films exhibit resistivity of order of $7.1–3.4\times10^{-1}$ Ω cm [16].

Temperature dependence of electrical resistivity is an important aspect to explore. Fig. 6 shows variation of log ρ versus reciprocal of temperate (T) for all the samples. The plot shows two distinct regions having different slopes, corresponding to low temperature region (region-I) and high temperature region (region-II). In region-I, the resistivity (ρ) is almost constant up to 340 K after which it decreases rapidly with rise in temperature of the sample up to 575 K. The donor activation energy values are shown in Table 1. The existence of two regions is reported by Vishwakarma et al. [22] for CVD films. The decrement in resistivity of the samples with temperature is due to decrement in grain boundary

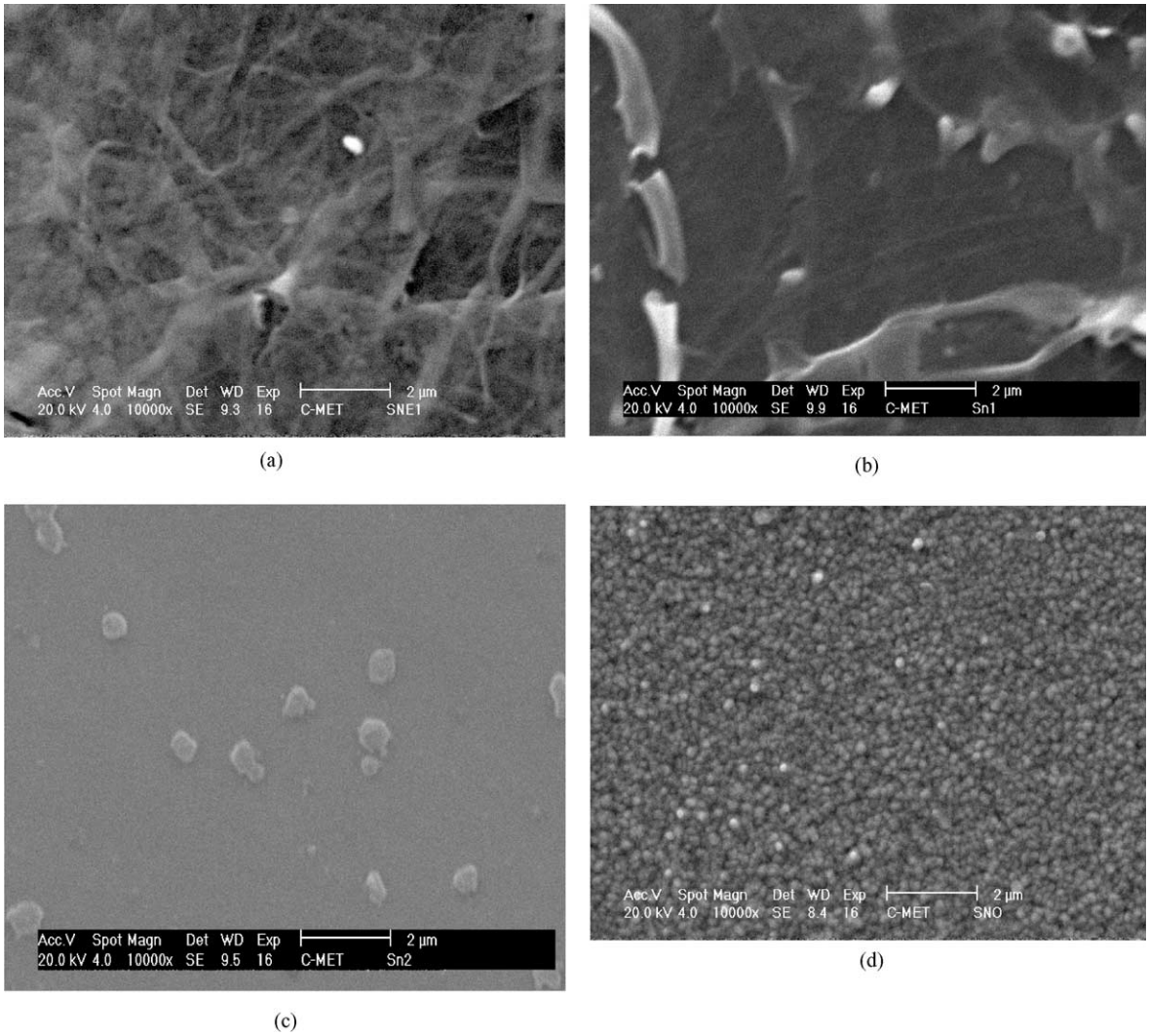

Fig. 5. Scanning electron micrographs (SEMs) of the samples of tin oxide thin films deposited at various substrate temperatures, S1 (300 °C), S2 (350 °C), S3 (400 °C) and S4 (450 °C).

concentration [11] and increment in oxygen vacancies [13], which enhance carrier concentration and mobility of the charge carriers.

Typical values of carrier concentration (n) and mobility of the charge carriers for the spray deposited SnO_2 films are reported to be about 2.7×10^{19} cm^3 and 6 cm^2 V^{-1} s^{-1} for 300 °C and 1.2×10^{18} cm^3 and 15 cm^2 V^{-1} s^{-1} for 450 °C, respectively [18,21]. The activation energy values in region I indicate the presence of a shallow donor levels near the bottom of the conduction band, where as the presence of activation energy in region-II indicates presence of deep donor levels, which might have resulted from defects and impurities such as iron and chromium. Generally, the films grown by spray pyrolysis are reported to consist of iron and chromium impurities, which cannot be totally alleviated [15].

3.7. Thermo-electric power measurement

Thermo-electric power (TEP) is the ratio of thermally generated voltage to the temperature difference across the semiconductor. This gives the information about charge carriers in the given material. For tin oxide material, conduction electrons originate from ionized defects such as oxygen vacancies. TEP of all the samples was studied in the temperature range 300–575 K using TEP unit with alumel-chromel thermocouple with ±5 K accuracy. Thermally generated electrons in the semiconductor always migrate from hot end to cold end. The polarity of thermally generated voltage at the hot junction was positive indicating that the films exhibit n-type conductivity. The variation of the thermo emf with temperature difference (ΔT) for all the samples is shown in Fig. 7. From the plot, it is observed that thermo emf increases almost linearly with increase in the temperature difference. The magnitude of TEP decreases with increase in deposition temperature, which may be attributed to the amelioration of crystallinity, due to which intergranular barrier height decreases. The values of thermo-electric power (TEP) lie in the range of 16–45 μV/°C and the values are listed in Table 1. It has been frequently reported in the literature that as the carrier concentration in SnO_2 increases, TEP decreases and TEP continues to increase with increasing temperature [22].

In our investigation, we have anticipated that due to asperity and relatively poor crystallinity sample S1 has low carrier concentration, due to which TEP in this sample has large value in the studied temperature range. As films become smooth and crystalline in order of S2, S3 and S4, TEP values subsequently decease thereby

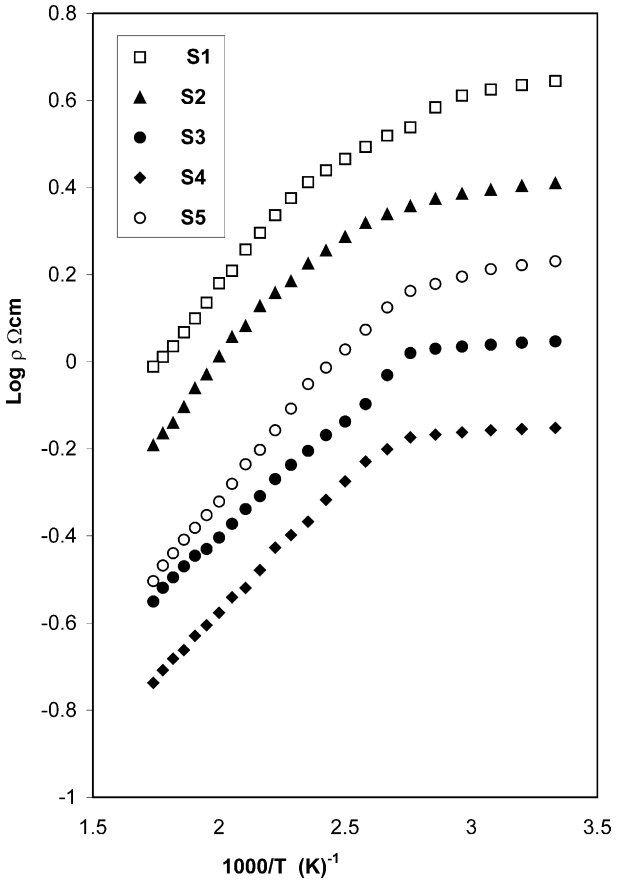

Fig. 6. The variation of log ρ versus (1000/T) for all the samples of tin oxide thin films deposited at various substrate temperatures, S1 (300 °C), S2 (350 °C), S3 (400 °C), S4 (450 °C) and S5 (500 °C).

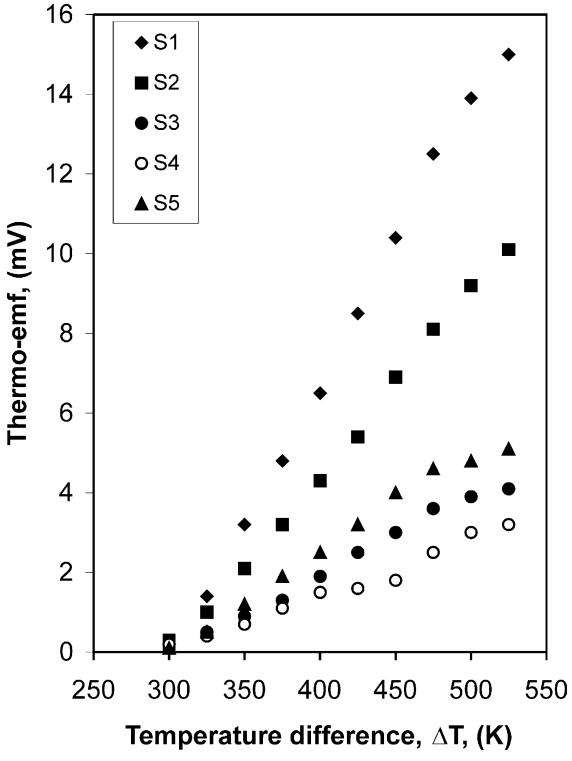

Fig. 7. The variation of thermo-emf (mV) versus temperature difference, ΔT, (K) for all the samples of tin oxide thin films deposited at various substrate temperatures, S1 (300 °C), S2 (350 °C), S3 (400 °C), S4 (450 °C) and S5 (500 °C).

convincing the above effect. It is interesting to note that the TEP values for sample S5 are lower than samples S1 and S2 and higher than that of samples S3 and S4. This indicates that although, sample S5 exhibits better crystallinity, as it is approaching towards stoichiometric SnO_2, carrier concentration, resulting from oxygen vacancies, decreases thereby incrementing the TEP values, deferring from the trend.

3.8. Optical properties

It is well known that SnO_2 is a degenerate semiconductor with band gap energy (*Eg*) in the range of 3.4–4.6 eV [9,14]. This scatter in band gap energy (*Eg*) of SnO_2 may be due to varied extent of non-stoichiometry of the deposited layers. The dependency of the band gap energy on the carrier concentration has been explicitly given in the literature [14]. It has been apprehended that band gap energy increases linearly with the increase in carrier concentration to the power 2/3.

Fig. 8 shows the variation of $(\alpha h\nu)^2$ versus $h\nu$ for all the samples. The nature of the plots indicates the existence of direct optical transitions. The band gap (*Eg*) is determined by extrapolating the straight-line portion of the plot to the energy axis. The intercept on energy axis gives the value of band gap energy *Eg* for all the samples and the values lie in the range of 3.62–3.87 eV and are given in Table 1. It is noticed that band gap energy

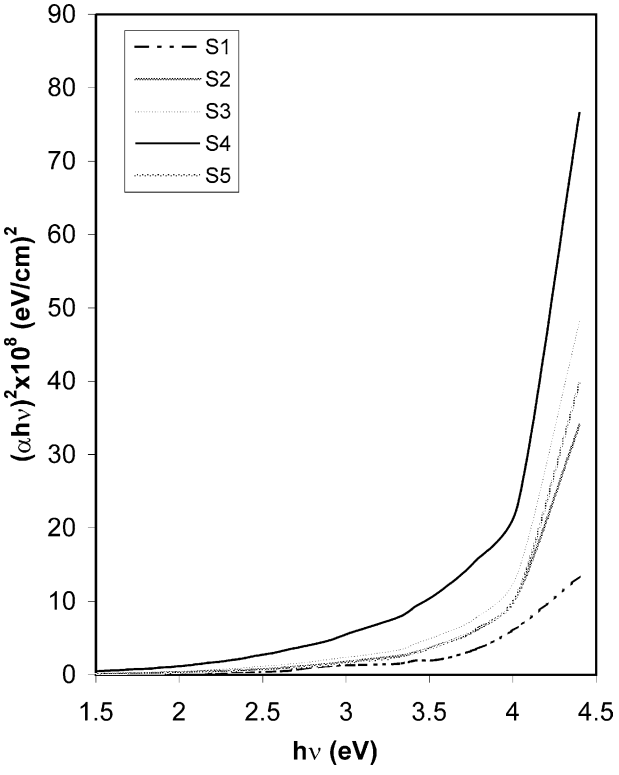

Fig. 8. The variation of $(\alpha h\nu)^2$ versus $h\nu$ for all the samples of tin oxide thin films deposited at various substrate temperatures, S1 (300 °C), S2 (350 °C), S3 (400 °C), S4 (450 °C) and S5 (500 °C).

value is minimum (3.62 eV) for sample S1, amongst all other samples, owing to lower carrier concentration. It increases gradually and attains maximum (3.87 eV) for sample S4, carrier concentration being higher for sample S4. As carrier concentration is higher, absorption of the light by the carriers also increase, leading to higher absorption coefficient (α) in the sample S4. As carrier concentration decreases, absorption by the carriers also decreases, resulting into lower α values in other samples. For sample S5, the band gap energy value slightly decreases to 3.85 eV.

The constituents of valance and conduction band in SnO_2 have been described by Munnix and Schmeits [26]. The width of the valance band is about 9 eV, which has been segmented in three different regions resulting from, (i) coupling of Sn *s* orbitals and O *p* orbitals, (ii) mingling of O *p* orbitals with smaller fraction of Sn *p* orbitals and (iii) mainly O *p* lone pair orbitals. The Sn *s* states mainly contribute to the formation of bottom of conduction band and top of conduction band has dominated Sn *p* character. The above discussion is clear enough to understand $s \rightarrow p$ direct optical transition in SnO_2 thin films. Our result also matches well with above discussion hence we conclude that in spray deposited undoped SnO_2 film direct $s \rightarrow p$ optical transitions prevail.

The transmittance of all the samples was measured in the wavelength range 300–850 nm using UV–vis-NIR spectrophotometer. The observed transmittance of all the samples at 630 nm was listed in Table 1. From the values, sample S5 shows maximum (85%) transmittance among the samples. It is also observed that the transmittance increases with the substrate temperature.

4. Conclusions

The simple and inexpensive spray pyrolysis technique was used to prepare thin films of tin oxide onto the amorphous glass substrates. During spray deposition, pyrolytic decomposition of $SnCl_4 \cdot 5H_2O$ precursor solution at the substrate temperatures 300–450 °C leads to the formation of non-stoichiometric tin oxide. Samples prepared at 500 °C appear to be nearly stoichiometric. It is observed from DTA and TGA studies that the complete pyrolytic decomposition of the precursor takes place at about 700 °C, leading to stoichiometric SnO_2. The existence of Sn–O and Sn–O_2 bands were confirmed from IR and Raman Spectra. The O/Sn ratio was estimated to be about 1.7 for the samples deposited above 350 °C and 1.6 for those deposited below it. The XRD studies revealed that all the films are polycrystalline in nature and crystallinity and grain size ameliorates with increase in substrate temperature. The room temperature electrical resistivity of all the samples lies in the range of 4.4–0.7 Ω cm. Sample S4 exhibits lowest ρ_{RT}

(0.7 Ω cm). The n-type conductivity was confirmed from the thermoelectric power measurements. The optical direct band gap lies in range between 3.62 and 3.87 eV.

Acknowledgements

The authors (P.S.C., R.K.K.) gratefully acknowledge U.G.C., New Delhi, India for the award of Teacher Fellowship under IXth plan. The authors acknowledge financial support from U.G.C.-D.R.S. (S.A.P.) project. The authors are thankful to Professor A. Ramam, I.M.R.E., Singapore for carrying out Raman Spectroscopy.

References

[1] J. Isidorsson, C.G. Granqvist, Solar Energy Mater. Solar Cells 44 (1996) 375.
[2] S. Samson, C.G. Fonstad, J. Appl. Phys. 44 (1973) 4618.
[3] K.L. Chopra, S. Major, D.K. Pandya, Thin Solid Films 102 (1983) 1.
[4] C.G. Granqvist, Handbook of Inorganic Electronic Materials, Elsevier Publication, The Netherlands, 1995.
[5] B. Stjerna, E. Olsson, C.G. Granqvist, J. Appl. Phys. 76 (1994) 3797.
[6] J.C. Manifacier, J.P. Fillard, Thin Solid Films 77 (1981) 67.
[7] B. Orel, D. Lavrencic- Stanger, K. Kalcher, J. Electrochem. Soc. 141L (1994) 127.
[8] P. Olive, E.C. Pereira, E. Longo, J.A. Varela, L.O. de, S. Buthoes, J. Electrochem. Soc. 140L (1993) 81.
[9] A. Czapla, E. Kusior, M. Bucko, Thin Solid Films 182 (1989) 15.
[10] E. Leja, J. Korecki, K. Krop, K. Toll, Thin Solid Films 59 (1979) 147.
[11] D. Das, R. Banerjee, Thin Solid Films 147 (1981) 321.
[12] S. Shanthi, C. Subramanium, P. Ramasamy, Mater. Sci. Eng. B57 (1999) 127.
[13] J. Bruneaux, H. Cachet, M. Froment, A. Masssad, Thin Solid Films 197 (1991) 129.
[14] A.E. Rakshani, Y.H.A. Makdisi, Ramazanyan, J. Appl. Phys. 83 (1998) 1049.
[15] V. Vasu, A. Subrahmanyam, Thin Solid Films 202 (1991) 283.
[16] M. Fantini, I. Torriani, Thin Solid Films 138 (1986) 255.
[17] C. Agashe, M.G. Takwale, B.R. Marathe, V.G. Bhide, Solar Energy Mater. 17 (1988) 99.
[18] E. Shanthi, V. Datta, A. Banerjee, K.L. Chopra, J. Appl. Phys. 51 (1980) 6243.
[19] E. Shanth, V. Datta, A. Banerjee, K.L. Chopra, Thin Solid Films 88 (1982) 93.
[20] T.D. Senguttuvan, L.K. Malhotra, Thin Solid Films 289 (1996) 22.
[21] N.S. Murti, G.K. Bhagwat, S.R. Jawalekar, Thin Solid Films 92 (1982) 347.
[22] S.R. Vishwakarma, J.P. Upadhyay, H.C. Parsad, Thin Solid Films 176 (1989) 99.
[23] M. Fujimoto, T. Urano, S. Marai, Y. Nishi, Jpn. J. Appl. Phys. 28 (1989) 2587.
[24] P. Scherrer, Gottinger, Nachr. 2 (1918) 98.
[25] L. H. Vlack, Elements of Materials Science, Adison-Wesley Publication, 1959, p. 98.
[26] S. Munnix, M. Schmeits, Phys. Rev. B 27 (1983) 7624.